

Electric vehicle battery parameter identification and SOC observability analysis: NiMH and Li-S case studies

 ISSN 1755-4535
 Received on 27th September 2016
 Revised 20th May 2017
 Accepted on 2nd July 2017
 E-First on 27th July 2017
 doi: 10.1049/iet-pel.2016.0777
 www.ietdl.org

 Abbas Fotouhi¹ ✉, Daniel J. Auger¹, Karsten Propp¹, Stefano Longo¹
¹School of Aerospace, Transport and Manufacturing, Cranfield University, Cranfield MK43 0AL, UK

✉ E-mail: a.fotouhi@cranfield.ac.uk

Abstract: In this study, battery model identification is performed to be applied in electric vehicle battery management systems. Two case studies are investigated: nickel-metal hydride (NiMH), which is a mature battery technology, and lithium-sulfur (Li-S), a promising next-generation technology. Equivalent circuit battery model parameterization is performed in both cases using the Prediction-Error Minimization algorithm applied to experimental data. Performance of the Li-S cell is also tested based on urban dynamometer driving schedule (UDDS). The identification results are then validated against the exact values of the battery parameters. The use of identified parameters for battery state-of-charge (SOC) estimation is also discussed. It is demonstrated that the set of parameters changes with a different battery chemistry. In the case of NiMH, the battery open circuit voltage (OCV) is adequate for SOC estimation whereas Li-S battery SOC estimation is more challenging due to its unique features such as flat OCV-SOC curve. An observability analysis shows that Li-S battery SOC is not fully observable and the existing methods might not be applicable for it. Finally, the effect of temperature on the identification results and the observability are discussed by repeating the UDDS test at 5, 10, 20, 30, 40 and 50 degree Celsius

1 Introduction

Road vehicles are becoming increasingly electrified. One of the most significant issues of the development of electric vehicles (EVs) is energy storage technology. Batteries, as the most common type of energy storage systems, may have different electrochemical features depending on their exact chemistry, and they may need to be managed in different ways. In the literature, many battery chemistries have been investigated and used for automotive applications: lead-acid, nickel-metal hydride (NiMH), and lithium-ion (Li-ion) are just a few examples. There is much research on improved battery technologies with many aims such as increasing battery capacity, lower cost and greater safety. Among these new battery technologies, lithium-sulphur (Li-S) can be a promising technology with higher specific energy (up to 650 Wh/kg in theory [1]). This offers the potential for increased energy storage capacity without an increase in weight. Good explanations of the electrochemical reactions taking place inside a Li-S battery can be found in the literature [2–5] and are not duplicated here. Li-S technology has developed dramatically, though it has not yet been deployed in a full-scale EV to date mainly due to its insufficient power output and lifetime. Part of efforts to bring it to market is the development of battery management algorithms to get the most out of Li-S and manage its state effectively.

There are many studies in the literature focusing on development of battery modelling and estimation techniques for various battery types. Battery modelling techniques, reviewed in [6], include analytical, electro-chemical and electrical circuit modelling approaches whereas battery state estimation techniques, reviewed in [7, 8], contains a wide range of algorithms such as coulomb counting, look-up tables or polynomials and recursive adaptive filters [9–13] which are particularly used for automotive application as well [14–17]. The proposed techniques in the literature have been mostly applied for lead-acid, NiMH and Li-ion batteries, however, there is no similar study focusing on Li-S battery since it is a roughly new technology and it is still under development.

In this study, a primary discussion on Li-S cell parameterisation and state estimation is presented. Indeed, a problem is detected and analytically discussed; however, the final solutions are left for further studies in this area. Based on an observability analysis

performed in this study, it is shown that the existing battery state estimation methods might not be applicable for Li-S battery chemistry because of its unique features. Two case studies are investigated here: NiMH and Li-S. The NiMH battery chemistry is selected as it is a mature battery technology which has been the subject of many previous studies. It is also ‘safe’, and therefore suitable for an experimental laboratory environment. As might be expected, the second chemistry is Li-S. For application in EVs, an ‘equivalent circuit’ modelling approach is chosen which is fast enough for real-time applications. Experimental tests are carried out in order to parameterise the battery models under different working conditions. Two types of experimental tests were performed: a typical pulse test and a more realistic test based on urban dynamometer driving schedule (UDDS). An observability analysis is then performed for battery state-of-charge (SOC) estimation which contains novel results about Li-S battery in comparison to NiMH and Li-ion.

This paper is structured as follows. Battery model identification is presented in Section 2 including equivalent circuit modelling of NiMH and Li-S batteries, battery experiments, model parameterisation algorithm and evaluation of the proposed framework under real driving condition. In Section 3, battery SOC observability analysis is performed for both cases, NiMH and Li-S. Challenges of the Li-S battery modelling and estimation due to its unique features are discussed and a potential solution is also discussed. The outcomes are then summarised in Section 4.

2 Battery model identification

2.1 Battery equivalent circuit modelling

Electrical circuit modelling or equivalent circuit network (ECN) modelling is a common method for simulating battery performance. Having less complexity than high-fidelity electrochemical models, ECN models have been used in a wide range of applications and for various battery types [18–21]. ECN battery models are constructed by putting resistors, capacitors and voltage sources in a circuit. Schematic diagram of an equivalent circuit battery model, called ‘Thevenin’ model [22, 23] or one RC network model (1RC model), is illustrated in Fig. 1. In this model, V_t is the battery's terminal voltage, V_{OC} is the battery's open circuit

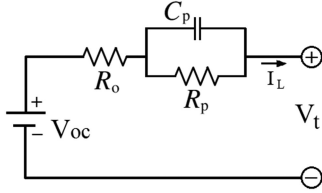


Fig. 1 Thevenin battery model (1RC model)

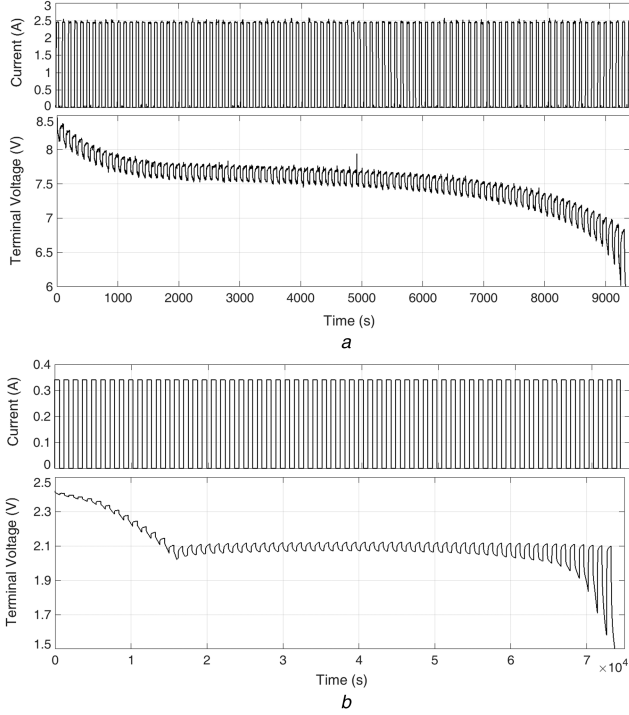


Fig. 2 Battery measurements
(a) NiMH, (b) Li-S

Table 1 NiMH battery pack and Li-S cell specifications

Battery chemistry	NiMH	Li-S
rated capacity, mAh	2400	3400
number of cells	6	1
rated voltage, V	7.2	2.1
full-charged voltage, V	8.5	2.4
cut-off voltage, V	6	1.5

voltage (OCV), R_O is the battery's ohmic resistance, and R_P and C_P are equivalent polarisation resistance and capacitance, respectively. The dynamic equations of the Thevenin model are as follows:

$$\begin{cases} V_t = V_{OC} - R_O I_L - V_P \\ \frac{dV_P}{dt} = -\frac{1}{R_P C_P} V_P + \frac{1}{C_P} I_L \end{cases} \quad (1)$$

2.2 Battery experiments

The batteries studied here are a six-cell NiMH battery pack, and a single Li-S cell developed by OXIS Energy Ltd [1]. Technical specifications of both batteries are presented in Table 1. The test bench which was used for NiMH battery experiments is explained in [24]. For Li-S cell experiments, a Maccor Series-4000 battery tester was used. The battery tester is a voltage/current device that applies a current and measures the voltage or vice versa. The cell is contained inside an aluminium test box inside a thermal chamber to set the desired temperature during each test. In both case studies (NiMH and Li-S), experiments are conducted by applying consecutive discharge current pulses to the battery and measuring

terminal voltage as the output. Each test starts from fully charged state and continues until the terminal voltage drops below the cut-off voltage (presented in Table 1) that means depleted charge state. In Fig. 2, battery measurements including current and terminal voltage, which are recorded at 25°C, are shown for two tests on NiMH and Li-S.

2.3 Battery parameter identification algorithm

In the proposed approach, a system identification technique is used to find the battery parameters based on input–output battery measurements which are current and terminal voltage. Different algorithms can be used to fit a battery model to the experimental data. The choice of a suitable fitting algorithm depends on the complexity of the battery model and computational effort limitations as discussed in [25]. It is concluded in [25] that prediction-error minimisation (PEM) algorithm is a proper algorithm for battery model parameterisation in this case.

In the identification procedure, the model's parameter vector θ is determined so that a prediction error, $\epsilon(t_k, \theta)$, is minimised as follows:

$$\epsilon(t_k, \theta) = y(t_k) - \hat{y}(t_k|t_{k-1}; \theta) \quad (2)$$

where $y(t_k)$ is the measured output at time k and $\hat{y}(t_k|t_{k-1}; \theta)$ is predicted value of the output at time k using the parameters θ . The prediction error depends on the parameter vector, so an iterative minimisation procedure has to be applied. Consequently, a scalar fitness function is minimised as follows:

$$E_N(\theta) = \det \left(\frac{1}{N} \sum_{k=1}^N \epsilon(t_k, \theta) \epsilon^T(t_k, \theta) \right) \quad (3)$$

For the model shown in Fig. 2, the parameters vector has four elements as follows. The parameters are optimised so that the least difference between measured terminal voltage and model's output is achieved

$$\theta = [R_O, V_{OC}, R_P, C_P] \quad (4)$$

$$\epsilon(t_k, \theta) = V_t(t_k) - \hat{V}_t(t_k|t_{k-1}; \theta) \quad (5)$$

Both NiMH and Li-S models are identified using PEM algorithm based on the experimental data presented in the previous section.

2.4 Battery parameter identification results

The parameters of the 1RC model are obtained for both NiMH and Li-S cases using PEM algorithm. The identification process is repeated over the whole range of SOC at regular intervals called 'identification window'. This can be a time window or SOC window. However, a combination of both is designed and used in this study, suitable for EV application. Since the power demand from an EV's battery pack can change in a wide range, identification at regular time intervals is not effective. On the other hand, EV battery's SOC can change in few seconds when the power demand is very high. This may cause numerical problems for the identification process when the number of the data points is not enough to identify the parameters. Here, the identification process is repeated every 1% change in SOC. So, the battery model is identified using the measurement's history in the past 1% SOC. However, the identification window's length is extended to the past 2 min when it is less than that.

Identified values of the battery parameters are illustrated in Fig. 3 for NiMH and Li-S. Fig. 3a shows that the OCV–SOC curve of NiMH battery is a very smooth curve with always positive gradient which makes it suitable for SOC estimation. The ohmic resistance is sensitive to SOC variation just at low and very high SOC levels, however this sensitivity is less in the middle. The NiMH battery polarisation resistance is almost flat in a wide range of SOC between 20 and 80% which means that it is not suitable for SOC estimation at all. The polarisation capacitance is the most

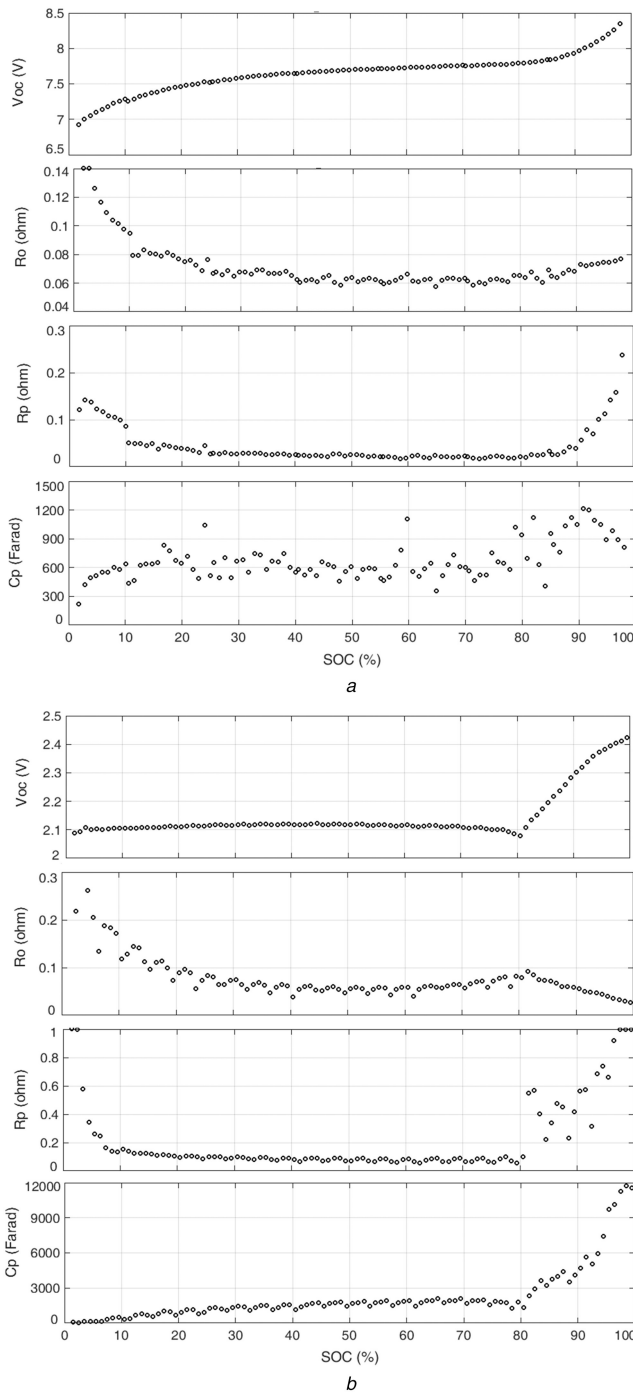


Fig. 3 Identified values of Thevenin battery model's parameters
(a) NiMH, (b) Li-S

difficult to identify and the fluctuation makes it unsuitable to be used for SOC estimation. On the other hand, Fig. 3b shows completely different results for the Li-S cell. The main difference is the OCV–SOC curve which is flat for Li-S in a wide range. In Section 3, an observability analysis is performed showing the differences between the two battery types using a mathematical representation. The results presented in Fig. 3 are obtained for a typical discharge pulse test. Since this study is focused on EV application, a more realistic test was also conducted based on EV simulation over a drive cycle discussed in the following part.

2.5 Battery parameter identification under real driving condition

In a case study, performance of the proposed battery parameter identification algorithm is evaluated in a more realistic scenario for EV application. For this purpose, an experimental test was performed based on EV power demand on UDDS, also known as

Table 2 Numerical values of EV model parameters

Parameter	Description	Value	Unit
A_f	vehicle frontal area	2.27	m ²
C_d	drag coefficient	0.29	—
C_r	rolling resistance coefficient	0.012	—
$F_{b f, \max}$	maximum brake force	3500	N
g	gravity	9.81	m/s ²
G	gear ratio	7.94	—
M_v	vehicle mass	1685	kg
R_w	wheel's radius	0.31	m
ρ	air density	1.225	kg/m ³
η_m	electric motor's efficiency	0.88	—
η_{gear}	gearbox efficiency	0.97	—
γ_{regen}	regeneration efficiency	0.3	—

U.S. FTP-72 (Federal Test Procedure) [26]. As the input of these tests, a typical EV model was developed based on Nissan LEAF specifications. The EV model was built using MATLAB/Simulink according to Nissan LEAF specifications presented in Table 2 [27, 28].

A proportional–integral controller was used as the driver model to follow a drive cycle. The controller's gains were tuned using Ziegler–Nichols method. At each simulation time step, vehicle's velocity is compared with the driving cycle and a velocity tracking error is calculated. Regarding the velocity error, driver's acceleration/brake command is generated. EV traction force is then calculated based on vehicle's dynamical equations. The required power signal is sent to EV's battery pack. In the battery block, available power is calculated based on battery's voltage and current limitations. Finally, EV's traction force is calculated based on the deliverable power. Having the real traction force and all opposing forces (air drag, rolling resistance, road gradient and brake forces), vehicle's acceleration and speed are calculated.

After simulating the EV model over UDDS, the battery power demand was scaled-down to be applied to a single cell. Since, the Li-S cell used in this study is a prototype, it cannot deliver a high power in comparison to the existing Li-ion or NiMH cell in the market. This does not affect our results and conclusions because the final cells will have same characteristics curves in shape. Average power of a single Li-S cell which is used in this study is about 5 W. Assuming a maximum power demand of 60 kW in a typical EV to move based on UDDS drive cycle, 12,000 of these prototype Li-S cells are needed. Based on this calculation, the power demand from a single cell is obtained by dividing the EV power by the number of cells. The Li-S cell was tested using scaled-down current profiles obtained from the EV simulation. Like the pulse discharge test explained in Section 2.2, current and terminal voltage values were recorded at sampling rate of 1 Hz and at 30°C.

Fig. 4 shows a Li-S cell discharge test based on UDDS drive cycle. UDDS speed profile is illustrated at top. A scaled-down current profile is depicted in Fig. 4b which was applied to the Li-S cell. Each test was done by repeating the UDDS current profile from 100% SOC to depleted state as shown in Fig. 5a. Cell's terminal voltage was measured as the output of the system. PEM algorithm was used to parameterise the battery model during the UDDS test. Identified values of cell's parameters are shown in Fig. 5b. Time length of the test, which depends on the current profile and cell's capacity, was about 25 h in this case.

Important outcomes of Fig. 5 are: (i) the proposed real-time battery parameterisation technique is applicable in a real driving scenario as well, (ii) the two parameters, V_{OC} and R_O , are more robust against measurement noise and identification error. So, they are more useful for battery state estimation under driving condition in an EV. The reason is that the polarisation parameters, R_P and C_P , reflect the slower part of the battery's dynamic response in comparison to the ohmic resistance which reflects quick changes in the battery model's response (terminal voltage drop or jump) which

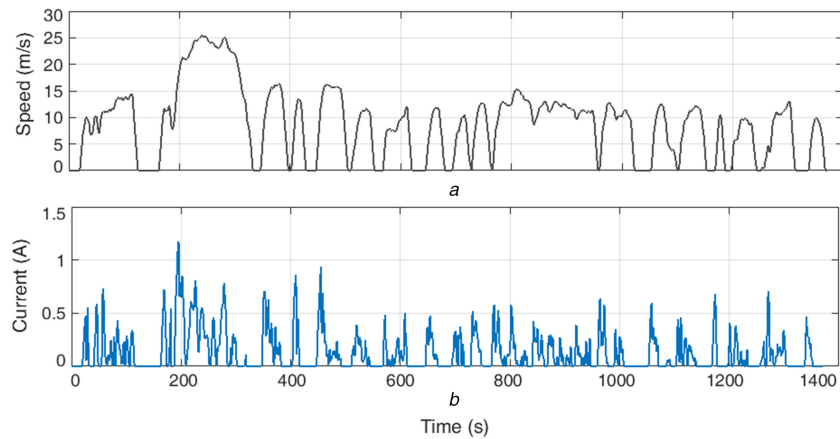


Fig. 4 Li-S cell discharge test based on UDDS drive cycle
(a) UDDS speed profile, (b) Li-S cell discharge current based on UDDS drive cycle

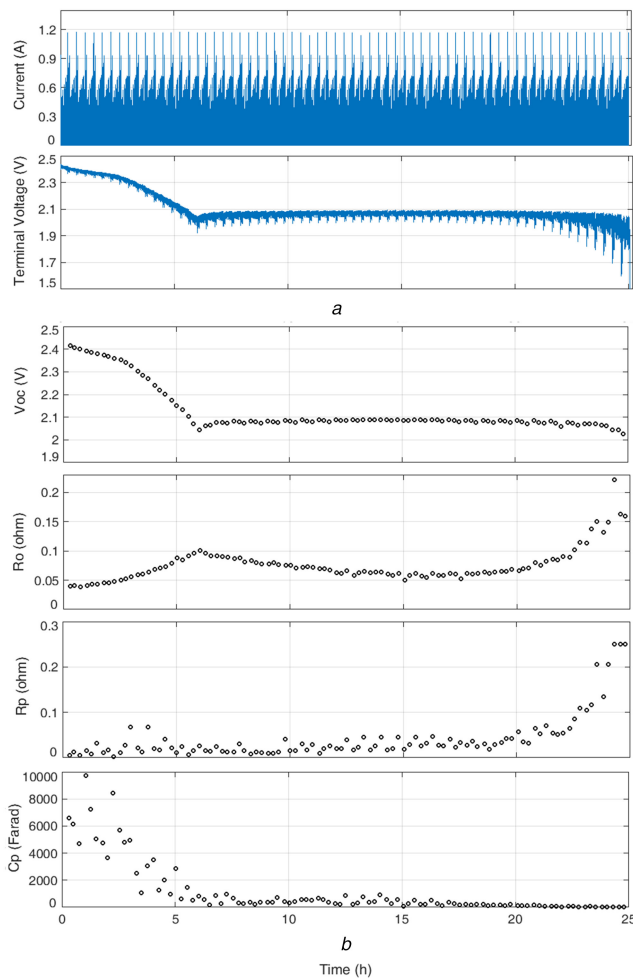


Fig. 5 UDDS Li-S cell test and parameterisation
(a) Discharge current and terminal voltage measurements, (b) Li-S cell model's parameters identified during UDDS test

usually happens under real driving condition. Another outcome is that the identification accuracy is a bit lower at very low SOC regions. The reason is not just relevant to the identification algorithm, but it is also due to the particular electrochemical reactions taking place inside a Li-S cell. There are completely different reactions taking place in a Li-S cell at various SOC levels [2–4]. This can lead to changes in this physical system (cell) to be identified. Based on our observations, this inconsistency in Li-S cell behaviour is more visible at very low SOC levels especially for internal resistance.

2.6 Battery parameter identification under mixed charge–discharge condition

In this section, the Li-S cell's behaviour subject to a charging pulse is also investigated. For this purpose, a new test was conducted including mixed charge–discharge pulses as shown in Fig. 6. In this test, various charge/discharge rates and different SOC levels are taken into consideration. The test started at full charge state (2.45 V) and continued to depletion when the cell's terminal voltage dropped below 1.5 V (i.e. the cut-off voltage). Consecutive charge/discharge current pulses were applied to the cell as shown in Fig. 6a. The pulse sequence consists of 18 pulses (nine discharge and nine charge pulses) covering different frequencies and amplitudes. As shown in Fig. 6b, the whole pulse sequence was applied ten times at ten charge levels to investigate SOC as well. Fig. 6b shows how the cell's terminal voltage has changed in response to the pulse sequence at different charge levels. A constant current (0.1 C) was applied to the cell between the pulse regimes in order to transfer the cell to another SOC level. Data was collected in the time domain with a sampling rate of 1 s. The measurements included time, current and cell's terminal voltage while temperature was monitored to ensure that it is being kept constant at 20°C.

Li-S cell model parameterisation was performed for each pulse sequence for charge and discharge pulses separately. Fig. 7 shows the most interesting outcome of this test which presents cell's ohmic resistance during charge and discharge. The results show that Li-S cell's ohmic charge resistance (OCR) is a bit more than ohmic discharge resistance (ODR) at very high SOC. This is something reasonable because cells do not tend to accept more charge at high SOC. Li-S cell's OCR and ODR are roughly equal around 85% SOC and after that, ODR becomes more and more as SOC decreases. Based on our results, the maximum difference between OCR and ODR of the Li-S cell is around 0.05 Ω happening at 4% SOC.

2.7 Identification results validation

In Section 2, battery model parameterisation was discussed using a system identification technique. The proposed technique was applied for NiMH and Li-S batteries under different experiments including discharge pulse test, UDDS test and mixed charge–discharge test. In all the case studies, parameters of a battery model were found in a way to minimise the difference between the model's output and the experimental measurements. Since the battery model's output is the terminal voltage, the error between the estimated and measured voltage is considered for evaluation of the identification results in this study. As the same procedure was used in all the case studies, the identification results validation is presented just for one case which is the mixed charge–discharge pulse test. Fig. 8 shows part of Li-S cell's terminal voltage measurement during the mixed charge–discharge test versus the identification results obtained from a 1RC model. The model has been parameterised using the identification technique explained in

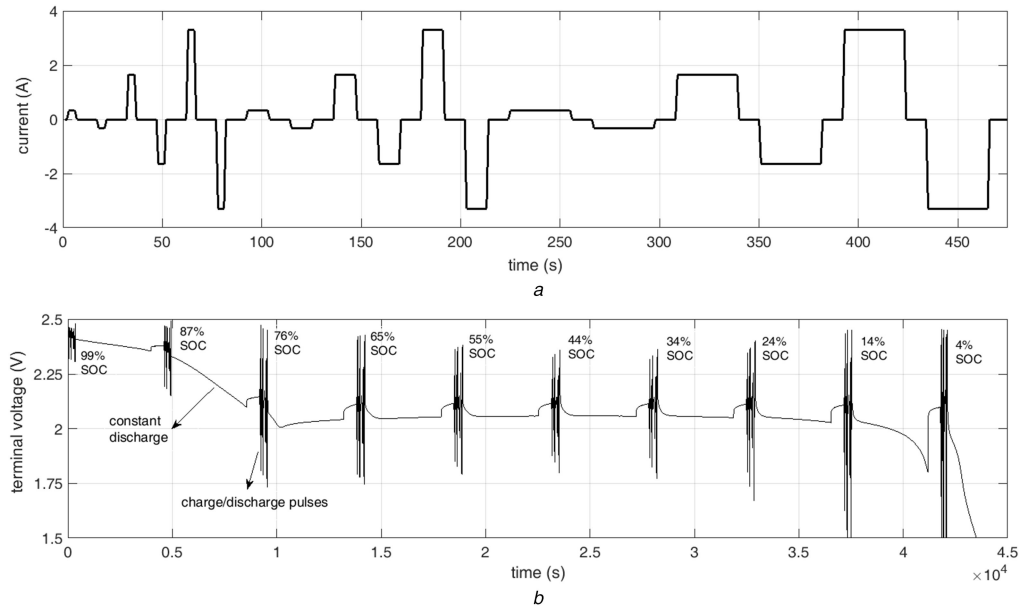


Fig. 6 *Li-S cell mixed charge–discharge test*
(a) Current pulse sequence, (b) Cell's terminal voltage

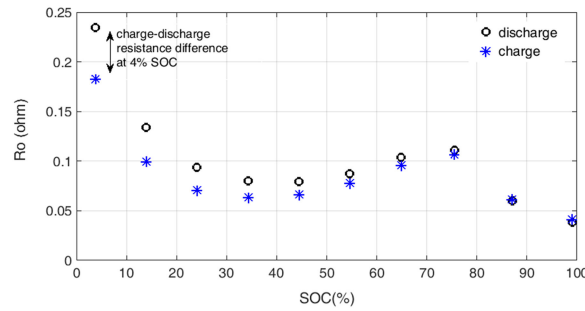


Fig. 7 *Li-S cell's ohmic resistance in charge and discharge versus SOC*

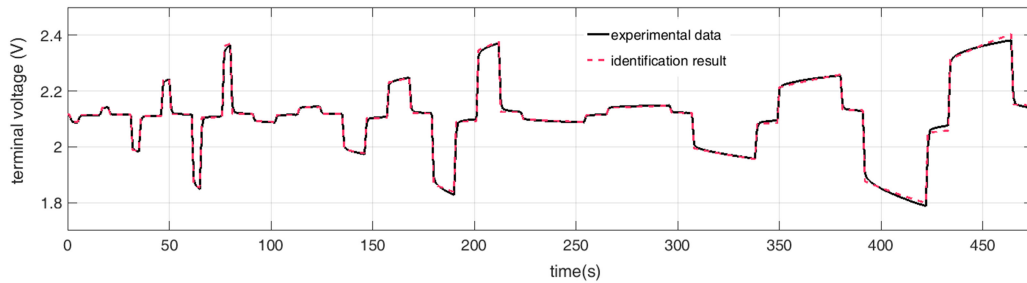


Fig. 8 *Measurement of Li-S cell's terminal voltage versus identification result*

Section 2.3. The difference between the identification results and the experimental measurements is calculated using a standard norm (L_2) as follows:

$$L_2 = \left[\frac{1}{N} \sum_{k=1}^N |e(t_k, \theta)|^2 \right]^{1/2} \quad (6)$$

where N is the number of measuring points (e.g. $N=475$ in Fig. 8 with a sampling time of 1 s), and the other parameters are same as explained in Section 2.3. The above error norm, called root mean square error (RMSE), was used to evaluate the identification accuracy. The RMSE value is obtained 7.29 mV for the test shown in Fig. 8 demonstrating the effectiveness of the proposed identification technique. Generally, the RMSE value depends on both the battery model structure (e.g. 1RC model) and the fitting algorithm. Using more complex model structures, like 2RC or 3RC, can improve the identification accuracy slightly, however, they are not suggested for real-time applications where the computational speed is also important [25].

3 Battery SOC observability analysis

3.1 Observability formulation

In this section, battery SOC observability is analysed for the two case studies, NiMH and Li-S. Referring to the battery differential equations in (1), an observability analysis would be possible if a state-space representation of the model is available in the standard form in below:

$$\begin{cases} \dot{x}' = Ax + Bu \\ y = Cx + Du \end{cases} \quad (7)$$

where x is the state vector, u is the input (i.e. current), y is the output (i.e. terminal voltage) and A , B , C and D are matrices that include battery model's parameters. Since the above state-space representation is obtained for linear systems, we need to linearise the non-linear battery model. For this purpose, a method which is presented in [29] is used here. In this method, V_P and SOC are considered as the model's states, current is the input and terminal

voltage is the output. For V_p , it is easy to write it in the standard state-space format, however, there is more to do for SOC. Using coulomb counting, SOC is calculated by integrating the load current to know how much capacity is used and remained. Assuming SOC_0 as the initial SOC at time t_0 , the battery's SOC at time t is defined as follows:

$$SOC = SOC_0 - \left(\int_{t_0}^t \frac{\eta i(\tau)}{C_t} d\tau \right), \quad 0 < SOC < 1 \quad (8)$$

where $i(t)$ is the current in ampere (A) and is assumed positive for discharging and negative for charging. Parameter η is the battery Coulombic efficiency and C_t is cell's total capacity in ampere-second (A s) when the time is in second. Therefore, SOC is a number between 0 and 1 representing depleted and fully-charged states, respectively.

There is still one term in the output equation that does not match with the standard form of state-space. OCV (V_{OC}) can be obtained as a non-linear function of SOC based on the identification results. Such a non-linear function can be divided into small linear parts using the gain scheduling method developed in [30]. Considering Δ_{SOC} as the SOC interval length, battery OCV can be written for the i th SOC interval as follows:

$$V_{OC} = a_i \cdot SOC_i + b_i \quad (9)$$

where $(i-1) \cdot \Delta_{SOC} \leq SOC_i \leq i \cdot \Delta_{SOC}$

The coefficients a and b are obtained from OCV–SOC curve and are constant at each small segment as illustrated in Fig. 9. So, OCV can be replaced by its linearised approximation in the output equation as follows:

$$V_t = a_i \cdot SOC + b_i - R_O I_L - V_p \quad (10)$$

Consequently, the state-space representation of the battery model is obtained as follows:

$$\begin{cases} \begin{bmatrix} \frac{dV_p}{dt} \\ \frac{dSOC}{dt} \end{bmatrix} = \begin{bmatrix} -\frac{1}{R_p C_p} & 0 \\ 0 & 0 \end{bmatrix} \begin{bmatrix} V_p \\ SOC \end{bmatrix} + \begin{bmatrix} \frac{1}{C_p} \\ \frac{\eta}{C_t} \end{bmatrix} I_L \\ V_t - b_i = [-1 \quad a_i] \begin{bmatrix} V_p \\ SOC \end{bmatrix} - R_O I_L \end{cases} \quad (11)$$

Having the model in state-space form, observability of the model can be analysed by calculating the observability matrix as follows [31]:

$$\mathbf{O} = \begin{bmatrix} C \\ CA \end{bmatrix} = \begin{bmatrix} -1 & a_i \\ \frac{1}{R_p C_p} & 0 \end{bmatrix} \quad (12)$$

The system is called observable if the above matrix is full rank.

3.2 Observability analysis results and discussion

Regarding the observability matrix obtained in the previous section, since R_p and C_p are positive non-zero numbers in the battery models, the only case in which the observability matrix is not full rank is when a_i be zero. This will never happen for the NiMH model because of the OCV–SOC characteristics for this battery type. However, the coefficient a_i might be zero for a Li-S battery as depicted in Fig. 9. Indeed, the results show that the system is not fully observable for the case of Li-S because of its unique features of OCV–SOC curve. This poor observability exists in the range of 20–70% SOC and can lead to many challenges in SOC estimation in this range. There are various battery SOC estimation methods in the literature, applied to different types of battery. A good review of these methods can be found in [7, 8].

The observability results in this study show that the existing battery SOC estimation methods in the literature might not be applicable for the Li-S battery. Most of the SOC estimation techniques are model based, which means they need a simplified battery model in forms of polynomials, look-up tables and so on. As shown in Fig. 9, the OCV curve of a Li-S cell can be divided into two regions (two plateaus) due to different electrochemical reactions taking place in each region [32]. From the control engineering point of view, this discontinuity and the poor observability in the range of 20–70% SOC, are two factors that make the Li-S battery SOC estimation problem more challenging than other battery types, needing particular considerations. The algorithms cannot easily converge to the true SOC if the initial condition is in the range of 20–70%. In addition, the discontinuity point can move to the right or to the left (inside the range of 70–85%) under different conditions. All these reasons make it challenging to model a Li-S cell precisely and consequently to estimate its SOC accurately.

Providing a solution for the above-mentioned problem is out of the framework of this study; however, mentioning to a potential solution might be useful here. In [33], a generic framework has been introduced for battery SOC estimation based on real-time battery model parameterisation. The main advantage of this technique is that there is no need to linearise the OCV–SOC curve like in the state-space model. The battery parameters are identified in real time and a non-linear mapping between the parameters and the battery SOC is constructed by an estimator. So, it is theoretically applicable to different types of battery including Li-S. Fig. 10 shows the whole structure of this framework, including battery measurements, parameter identification and SOC estimation units. The battery measurement consists of current (the controlled input) and terminal voltage (measured as an output), all in the time domain. The measurements are used by the identification unit to extract battery parameters in real time. The outputs of the identification unit (estimates of unknown parameters) are then used by the estimation unit to estimate the battery SOC. So before the online application, a non-linear mapping between the battery parameters and SOC should be found via an offline training process. The effect of temperature can also be taken into consideration in the estimation unit. Number and type of the outputs of the identification unit is not pre-determined: the number of parameters is chosen based on what is required for an effective state estimation that also depends on the battery chemistry. In [33], performance of such a framework has been evaluated for NiMH battery SOC estimation. This idea might be extended in future studies for Li-S battery SOC estimation as well. In the case of NiMH, OCV can be used alone as an indicator of SOC, however, the situation is different for Li-S battery. Consequently, other battery parameters should be used by the estimator in case of Li-S.

The estimator unit in [33] is an adaptive neuro-fuzzy inference system (ANFIS) which estimates NiMH battery SOC using the identified value of OCV in real time. Generally, the idea is to find a non-linear mapping between the identification results and SOC by using a mapping function like f as below:

$$SOC = f(P_1, P_2, P_3, \dots) \quad (13)$$

where P_i is the i th identified battery parameter. As a designer, we are interested to use the minimum number of parameters in order to decrease the computational effort especially for online applications. Design of such a SOC estimator for Li-S battery can be more challenging since the OCV is not enough in this case. Fig. 9 shows that Li-S cell OCV can be used for SOC estimation in a specific range of SOC between 80 and 100%. In other words, we are sure about the SOC value when OCV is more than 2.12 V. In the range of <80% SOC, other parameters of the Li-S cell model might be used in addition like the ohmic resistance or even the polarisation resistance and/or capacitance.

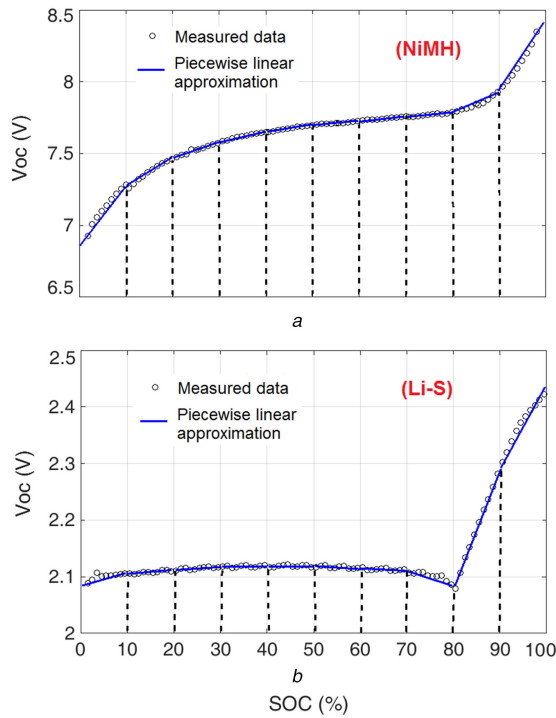


Fig. 9 Piecewise linear approximation of OCV-SOC curves
(a) NiMH, (b) Li-S

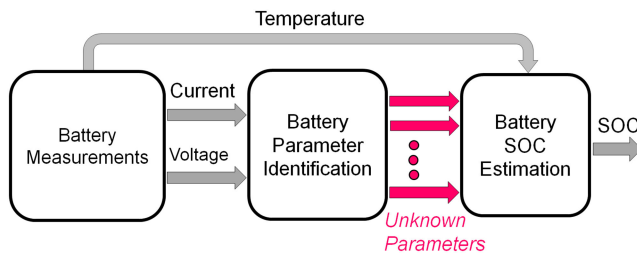


Fig. 10 Battery parameter identification for SOC estimation

4 Effect of temperature on Li-S cell parameterisation and SOC observability

The effect of temperature on battery's performance cannot be ignored for any type of battery. This topic has been addressed in many studies in the literature for different types of battery including NiMH. However, Li-S battery has been investigated less than other types due to its less availability in the market. For this reason, this section is allocated to just investigating the effect of temperature on our results presented in previous sections. The results show that especially for a Li-S cell, temperature has an intense effect on the cell's performance by changing the electrochemical reactions taking place inside the cell. The electrochemical discussions about this phenomenon are out of the scope of this paper and can be found in the literature [4]. From the control engineering point of view, we are interested to know how the temperature can affect the identification results and the observability analysis which is done in this study. For this purpose, a particular test on the Li-S cell has been repeated many times at different temperature levels. The UDDS test (introduced in Section 2.5) has been selected representing a real working condition for automotive application. The UDDS test was conducted at different temperature levels including 5, 10, 20, 30, 40 and 50°C as illustrated in Fig. 11. Two practical limits are applied in these tests: (i) the current profile was scaled down a bit in the test at 5°C in order to prevent hitting the cut-off voltage (1.5 V) at the breakpoint (around 75% SOC). The reason is the increase in resistance value at low temperature which is discussed in the following. For the other tests at 10, 20, 30, 40 and 50°C, the current profile is kept same as discussed in Section 2.5, and (ii) in order to prevent the shuttle phenomenon [34–36] at the end of charging, the cell was

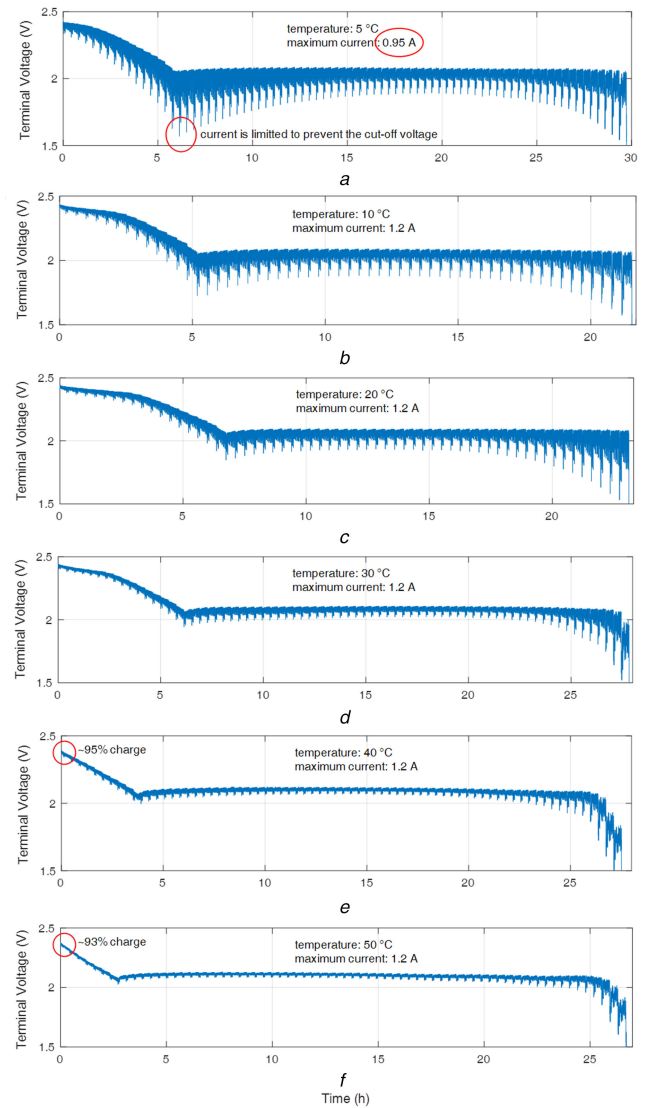


Fig. 11 Li-S cell's terminal voltage over the UDDS test at different temperature levels

charged up to 2.4 and 2.38 V (instead of 2.45) at 40 and 50°C, respectively. These upper bound voltages are equivalent to 95 and 93% SOC in comparison to other tests as shown in Fig. 11e and f.

As discussed in Section 2.5, the two parameters, OCV and ohmic resistance, are more reliable for SOC estimation. Fig. 12 shows the Li-S cell's ohmic resistance and OCV values which are identified over UDDS test at different temperature levels. Li-S cell's capacity is also calculated at different temperature levels as presented in Table 3. From these results, it is obvious that the temperature has a significant effect on the Li-S cell's parameters. This effect is clearer on the ohmic resistance even in a limited range of temperature variation. Based on the results presented in Fig. 12a, the maximum influence of the temperature variation on the ohmic resistance is observed around 75% SOC, exactly at the breakpoint between the two plateaus. The results are also showing a higher sensitivity to temperature variation at lower temperature levels. For example, variation of ohmic resistance when the temperature changes from 10 to 20°C is much more than the case in which it changes from 40 to 50°C. The resistance goes so high in case of 5°C that the same current profile is not applicable since the terminal voltage hits the cut-off voltage (1.5 V) at the end of high plateau as shown in Fig. 11a. In order to complete the test, the current profile is scaled down by factor of 0.8 in this case.

The effect of temperature on the OCV curve is shown in Fig. 12b. Although the temperature variation affects the OCV-SOC curve, this effect is not comparable to the resistance variations in Fig. 12a. Regarding the OCV curve only, the system remains unobservable at all temperature levels. However, the

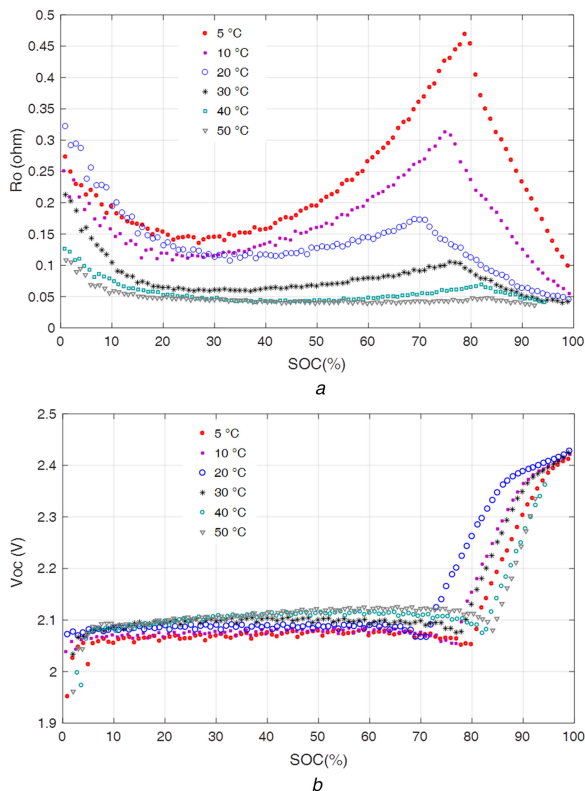


Fig. 12 Li-S cell's parameter identification during UDDS test at different temperature levels

Table 3 Effect of temperature on Li-S cell's capacity

Temperature, °C	Capacity, mAh
5	3021
10	2768
20	2927
30	3533
40	3486
50	3396

situation can get worst since the results show that the temperature not only affects the cell's resistance value, but also it changes the gradient of ohmic resistance versus SOC. This means that the observability analysis results are also affected by the temperature variation. In addition, the results show that Li-S cell's SOC observability improves at lower temperature since the gradient of the ohmic resistance versus SOC increases as the temperature decreases, which is desirable in the control point of view. On the other hand, if we have a look at the results in Table 3, it is clear that lower temperature means less capacity which is not desirable. Consequently, a proper trade-off is essential to find the optimal value of the temperature at which the Li-S cell has the best performance with regard to both capacity and observability.

The capacity values presented in Table 3 are obtained for the UDDS test with a maximum current of 1.2 A applied to a single cell. Generally, it is concluded that more capacity is available as temperature rises. In case of 5°C test, more capacity is measured than expected because a lower current is applied to the cell. For the tests done at 40 and 50°C, the measured capacity is not more than 30°C because the two tests were started from <100% SOC as discussed before. To compare the results and extract a mapping function between the capacity and the temperature, more tests are needed to be performed using the same current profiles. In addition, each test should be repeated at least three times to get more consistency in data by averaging the values. Assuming that each test takes around 40 h (charge and discharge) to complete, 1200 h testing is needed to cover ten different temperature levels which is left for our future work.

In a real application like an EV, it can be assumed that the EV battery pack's temperature in working condition is controlled by a battery management system in a limited range with an allowable deviation of $\pm 5^\circ\text{C}$ from a set point. However, our results show that design of a SOC estimator for Li-S battery is challenging even in a limited range of temperature variation. Although the effect of temperature on Li-S cell performance is discussed here briefly, we believe that more study is needed in this area. As a guideline for future studies, a potential solution might be training separate estimators to be used at different temperature levels in the framework shown in Fig. 10. In this approach, the whole temperature range of the working condition would be divided into a number of regions (e.g. n regions) and each estimator will be used in its particular range only.

5 Conclusions

In this study, Li-S cell ECN model parameterisation was performed under different conditions using the PEM identification algorithm. Various experimental tests were conducted on a 3.4 Ah Li-S cell including discharge pulse test, mixed charge–discharge pulse test and a test based on EV power demand on UDDS. Some of the experiments were also performed for a small NiMH battery pack to highlight the unique features of Li-S battery in comparison to other battery types. The identification results were validated against the experimental measurements showing a proper fitting between them (with a RMSE of 7.29 mV).

A SOC observability analysis was also performed for both case studies, NiMH and Li-S. The results show that the system is observable in the case of NiMH whereas it is not fully observable for Li-S because of its flat OCV–SOC curve. This poor observability exists in the range of 20–70% SOC and can lead to many challenges in SOC estimation. The observability analysis results in this study show that the existing battery SOC estimation methods in the literature might not be applicable for Li-S battery. The OCV curve of a Li-S cell can be divided into two regions (two plateaus) with a breakpoint in between. From the control engineering point of view, this discontinuity and the poor observability in the range of 20–70% SOC, are two factors that make Li-S battery SOC estimation problem more challenging than other battery types.

A potential solution was also discussed for estimation of Li-S cell's SOC. It was a generic framework for battery SOC estimation based on real-time battery model parameterisation. The main advantage of this technique was that there is no need to linearise the OCV–SOC curve like in the state-space model. The battery parameters are identified in real time and a non-linear mapping between the parameters and the battery SOC is constructed by an estimator like ANFIS. The method had been used for NiMH in the literature and is theoretically applicable to different types of battery including Li-S.

The effect of temperature on the Li-S cell's performance was also investigated. The results show that the temperature can significantly affect both Li-S cell's performance (capacity and power delivery) and observability. The results show a higher sensitivity to the temperature variation at lower temperature levels. However, Li-S cell's SOC observability improves at lower temperature since the gradient of the ohmic resistance versus SOC increases as the temperature decreases, which is desirable in the control point of view. On the other hand, lower temperature means less capacity which is not desirable. Consequently, a proper trade-off is essential to find the optimal value of the temperature at which the Li-S cell has the best performance and observability. The maximum effect of the temperature on Li-S cell's ohmic resistance was observed at the breakpoint between the two plateaus around 75% SOC. Although the effect of temperature on Li-S cell performance is discussed here briefly, we believe that more study is needed in this area.

This is an open research area, if it can be addressed; it increases the likelihood of realising the promise of Li-S as a next-generation battery technology.

5 Acknowledgments

This research was funded as part of the ‘Revolutionary Electric Vehicle Battery’ (REVB) project, co-funded by Innovate UK and EPSRC (TS/L000903/1 and EP/L505286/1), and the ‘Understanding Future Vehicles’ project funded by EPSRC (EP/I038586/1). Data underlying this study can be accessed through the Cranfield University repository at <http://dx.doi.org/10.17862/cranfield.rd.5172334>.

6 References

- [1] <http://www.oxisenergy.com>
- [2] Marinescu, M., Zhang, T., Offer, G.J.: ‘A zero dimensional model of lithium-sulfur batteries during charge and discharge’, *Phys. Chem. Chem. Phys.*, 2016, **18**, pp. 584–593
- [3] Neidhardt, J.P., Fronczek, D.N., Jahnke, T., *et al.*: ‘A flexible framework for modeling multiple solid, liquid and gaseous phases in batteries and fuel cells’, *J. Electrochem. Soc.*, 2012, **159**, (9), pp. 1528–1542
- [4] Wild, M., O’Neill, L., Zhang, T., *et al.*: ‘Lithium sulfur batteries, a mechanistic review’, *Energy Environ. Sci.*, 2015, **8**, pp. 3477–3494
- [5] Ghaznavi, M., Chen, P.: ‘Sensitivity analysis of a mathematical model of lithium-sulfur cells part I: applied discharge current and cathode conductivity’, *J. Power Sources*, 2014, **257**, pp. 394–401
- [6] Fotouhi, A., Auger, D.J., Propp, K., *et al.*: ‘A review on electric vehicle battery modelling: from lithium-ion toward lithium-sulphur’, *Renew. Sustain. Energy Rev.*, 2016, **56**, pp. 1008–1021
- [7] Ugras Cuma, M., Koroglu, T.: ‘A comprehensive review on estimation strategies used in hybrid and battery electric vehicles’, *Renew. Sustain. Energy Rev.*, 2015, **42**, pp. 517–531
- [8] Li, J., Barillas, J.K., Guenther, C., *et al.*: ‘A comparative study of state of charge estimation algorithms for LiFePO₄ batteries used in electric vehicles’, *J. Power Sources*, 2013, **230**, pp. 244–250
- [9] Zhong, L., Zhang, C., He, Y., *et al.*: ‘A method for the estimation of the battery pack state of charge based on in-pack cells uniformity analysis’, *Appl. Energy*, 2014, **113**, pp. 558–564
- [10] Liu, X., Chen, Z., Zhang, C., *et al.*: ‘A novel temperature-compensated model for power Li-ion batteries with dual-particle-filter state of charge estimation’, *Appl. Energy*, 2014, **123**, pp. 263–272
- [11] Schwunk, S., Armbruster, N., Straub, S., *et al.*: ‘Particle filter for state of charge and state of health estimation for lithium-iron phosphate batteries’, *J. Power Sources*, 2013, **239**, pp. 705–710
- [12] Zheng, C., Fu, Y., Mi, C.C.: ‘State of charge estimation of lithium-ion batteries in electric drive vehicles using extended Kalman filtering’, *IEEE Trans. Veh. Technol.*, 2013, **62**, (3), pp. 1020–1030
- [13] Rahimi-Eichi, H., Baronti, F., Chow, M.Y.: ‘Online adaptive parameter identification and state-of-charge coestimation for lithium-polymer battery cells’, *IEEE Trans. Ind. Electron.*, 2014, **61**, (4), pp. 2053–2061
- [14] He, W., Williard, N., Chen, C., *et al.*: ‘State of charge estimation for electric vehicle batteries using unscented Kalman filtering’, *Microelectron. Reliab.*, 2013, **53**, (6), pp. 840–847
- [15] Plett, G.L.: ‘Extended kalman filtering for battery management systems of LiPB-based HEV battery packs: part I. Background’, *J. Power Sources*, 2004, **134**, pp. 252–261
- [16] Plett, G.L.: ‘Sigma-point Kalman filtering for battery management systems of LiPB-based HEV battery packs, Part 2: simultaneous state and parameter estimation’, *J. Power Sources*, 2006, **161**, pp. 1369–1384
- [17] Sun, F., Hu, X., Zou, Y., *et al.*: ‘Adaptive unscented Kalman filtering for state of charge estimation of a lithium-ion battery for electric vehicles’, *Energy*, 2011, **36**, (5), pp. 3531–3540
- [18] Marc, T., Oliver, B., Dirk, U.S.: ‘Development of a voltage-behavior model for NiMH batteries using an impedance-based modeling concept’, *J. Power Sources*, 2008, **175**, pp. 635–643
- [19] He, H., Xiong, R., Fan, J.: ‘Evaluation of lithium-ion battery equivalent circuit models for state of charge estimation by an experimental approach’, *Energies*, 2011, **4**, pp. 582–598
- [20] Brand, J., Zhang, Z., Agarwal, R.K.: ‘Extraction of battery parameters of the equivalent circuit model using a multi-objective genetic algorithm’, *J. Power Sources*, 2014, **247**, pp. 729–737
- [21] Hu, X., Li, S., Peng, H.: ‘A comparative study of equivalent circuit models for Li-ion batteries’, *J. Power Sources*, 2012, **198**, pp. 359–367
- [22] Salameh, Z.M., Casacca, M.A., Lynch, W.A.: ‘A mathematical model for lead-acid batteries’, *IEEE Trans. Energy Convers.*, 1992, **7**, (1), pp. 93–98
- [23] Mousavi G, S.M., Nikdel, M.: ‘Various battery models for various simulation studies and applications’, *Renew. Sustain. Energy Rev.*, 2014, **32**, pp. 477–485
- [24] Propp, K., Fotouhi, A., Auger, D.J.: ‘Low-cost programmable battery dischargers and application in battery model identification’. Proc. Computer Science and Electronic Engineering, Colchester, UK, 2015
- [25] Fotouhi, A., Auger, D.J., Propp, K., *et al.*: ‘Accuracy versus simplicity in online battery model identification’. *IEEE Trans. Man Syst. Cybern.*, 2016, **PP**, (99), pp. 1–12 DOI: 10.1109/TSMC.2016.2599281
- [26] <https://www.dieselnet.com/standards/cycles/ftp72.php>
- [27] Choi, G., Jahns, T.M.: ‘Design of electric machines for electric vehicles based on driving schedules’. Proc. IEEE Electric Machines and Drives, 2013, pp. 54–61
- [28] Hayes, J.G., de Oliveira, R.P.R., Vaughan, S., *et al.*: ‘Simplified electric vehicle power train models and range estimation’. Proc. IEEE Vehicle Power and Propulsion, 2011, pp. 1–5
- [29] Xu, J., Mi, C.C., Cao, B., *et al.*: ‘The state of charge estimation of lithium-ion batteries based on a proportional-integral observer’, *IEEE Trans. Veh. Technol.*, 2014, **63**, (4), pp. 1614–1621
- [30] Leith, D.J., Leithead, W.E.: ‘Survey of gain-scheduling analysis and design’, *Int. J. Control*, 2000, **73**, (11), pp. 1001–1025
- [31] Ogata, K.: ‘Modern control engineering’ (Prentice-Hall, Englewood Cliffs, NJ, USA, 2010, 5th edn.)
- [32] Ryu, H.S., Guo, Z., Ahn, H.J., *et al.*: ‘Investigation of discharge reaction mechanism of lithium/liquid electrolyte/sulfur battery’, *J. Power Sources*, 2009, **189**, (2), pp. 1179–1183
- [33] Fotouhi, A., Propp, K., Auger, D.J.: ‘Electric vehicle battery model identification and state of charge estimation in real world driving cycles’. Proc. Computer Science and Electronic Engineering, Colchester, UK, 2015, pp. 243–248
- [34] Hofmann, A.F., Fronczek, D.N., Bessler, W.G.: ‘Mechanistic modeling of polysulfide shuttle and capacity loss in lithium-sulfur batteries’, *J. Power Sources*, 2014, **259**, pp. 300–310
- [35] Moy, D., Manivannan, A., Narayanan, S.R.: ‘Direct measurement of polysulfide shuttle current: a window into understanding the performance of lithium-sulfur cells’, *J. Electrochem. Soc.*, 2015, **162**, (1), pp. A1–A7
- [36] Mikhaylik, Y., Akridge, J.: *J. Electrochem. Soc.*, 2004, **151**, (11), pp. 1969–1976

2017-07-06

Electric vehicle battery parameter identification and SOC observability analysis: NiMH and Li-S case studies

Fotouhi, Abbas

The Institution of Engineering and Technology

Fotouhi A, Auger DJ, Propp K, Longo S. (2017) Electric vehicle battery parameter identification and SOC observability analysis: NiMH and Li-S case studies. IET Power Electronics, Volume 10, Issue 11, 2017, pp. 1289-1297

<https://dspace.lib.cranfield.ac.uk/handle/1826/12228>

Downloaded from Cranfield Library Services E-Repository